


Ocean tides can drag the atmosphere and cause tidal winds over broad continental shelves

Lionel Renault ^{1,2}✉ & Patrick Marchesiello¹

Oceanic tides lead to some of the largest currents of the world ocean and have important implications for oceanic circulation. In the last decade, the feedback effect of surface currents on the overlying winds has been shown to strongly regulate the ocean circulation. Here we present evidence, using coupled high-resolution ocean-atmosphere simulations and in situ measurements, that ocean tides can drag the atmosphere above. The current-induced tidal winds expand across the atmospheric boundary layer, while dissipating tidal energy. They are likely present in many shelf regions of the world ocean, with an amplitude of about one-third of the underlying tidal currents, i.e., up to 1.5 ms^{-1} . Consideration of surface tidal winds can have implications in areas ranging from climate modeling to wind farming.

¹LEGOS, University of Toulouse, IRD, CNRS, CNES, UPS, Toulouse, France. ²Department of Atmospheric and Oceanic Sciences, University of California Los Angeles, Los Angeles, CA, USA. ✉email: lionel.renault@ird.fr

Ocean tides are mainly produced by the gravitational forces of the Sun and Moon and represent one of the main sources of energy of the world ocean¹. By affecting dissipation and mixing in the ocean, tides have a large effect on the general circulation and represent a major topic for oceanography^{1,2}. The direct gravitational effect of the Moon, characterized by a period of about 12.42 h, is the main tidal constituent in many locations (see e.g., Fig. 1a, b). In the past decades, satellite altimetry has been used to estimate the total rate of work done by tidal force, which represents 2.4 TW for the M2 tide out of 3.5 TW for all eight major constituents^{3,4}. How and where ocean tides dissipate is an important question, and it is now generally agreed that they dissipate primarily on continental shelves by bottom friction and by the dispersion of surface tides into internal waves by ocean topography^{5,6}.

Recently, air-sea interactions at the oceanic mesoscale (i.e., scales of 10–100 km and 10–100 days^{7–9}) have received a growing interest from the scientific community. In particular, the CFB (Current FeedBack) effect expresses the influence of surface ocean currents on the overlying atmosphere. CFB has two main direct effects on ocean circulation. At large scales, by reducing the mean energy input from the atmosphere to the ocean, it causes a slowdown in the mean ocean circulation^{10–12}. Second, the transfer of momentum from currents to winds also causes CFB to act as an eddy killer, reducing (sub)mesoscale activity by about 30%^{13–18}. As a result, CFB can reduce eddy-mean flow interactions, and thus partly control very energetic current systems such as western boundary currents^{19,20}. Ref. 20 demonstrate that CFB changes the usual conception of wind-driven currents. The wind can no longer be considered only as a large-scale energy source that triggers a turbulent cascade, as it can interact on a fine scale, directly affecting the whole oceanic spectrum.

In essence, CFB acts as a top drag²¹, which affects all spatial and temporal scales. In particular, tides should also be affected and some of their energy should be transferred to the atmosphere instead of being dissipated in the ocean. Tidal currents can interact with the overlying atmosphere, directly modifying surface stress and low-level winds. But surprisingly, the amount of energy that would be dissipated in this way and the effectiveness of this process in generating tidal winds are questions that have never been asked. Tidal winds are generally considered only as an S2 component in the upper atmosphere due to thermal heating rather than gravitational forces²², but never as a friction effect of oceanic tides. However, as we will see here, it may explain a diurnal frequency observed in surface observations such as over the English Channel (Fig. 1c).

To examine these issues, coupled eddy-rich ocean-atmosphere simulations are performed over the English Channel for the period 2010. The simulation set consists of two twin experiments that involve a control simulation with tides and CFB (CTRL) and an identical simulation without CFB (NOCFB). The comparison between the simulations will highlight the top drag effect on tides and will demonstrate the existence of a regime of tidal winds induced by tidal currents.

Results

The English Channel. The English Channel (Fig. 1a) separates Southern England from Northern France and is home to some of the strongest and most complex tides in the world. Figure 1b shows a spectral description of the sea surface height at the Bournemouth gauge (black star in Fig. 1a) compared to a regional simulation using the ocean model CROCO fully coupled with the atmospheric model WRF. Consistent with the literature, the English Channel, both in the observation and in the model, is affected by a wide range of tides, with M2 (12.42 h) being the

most energetic tidal constituent. CROCO shows good overall agreement with the data. The amplitudes of the main diurnal (K1), semi-diurnal (M2) and even nonlinear quarter- and sixth-diurnal tides are well reproduced by the model (while higher-frequency components of lesser importance appear over-estimated). For tidal currents, the M2 component of the model largely dominates the surface current spectrum as expected²³. Tidal currents can reach more than 3 m s⁻¹ near the coast and 2 m s⁻¹ in the middle of the Channel (Fig. 2a).

Ocean drag on the atmosphere. Figure 2a shows a snapshot of the zonal surface currents from CTRL, and Fig. 2b, a snapshot at the same time of surface stress anomaly estimated as the surface stress difference between CTRL and NOCFB, expressing the drag of the ocean on the atmosphere. Note that focus is done on the zonal component of the tidal current as it dominates the signal over this region (See Supplementary Fig. 2). On this broad, shallow continental shelf with little mesoscale ocean activity, the essential difference between the two simulations can be attributed to tides. The spatial pattern of the stress anomaly is very similar to that of surface currents. In agreement with the CFB effect found for lower frequency dynamics, tidal currents are anti-correlated with the surface stress response: a negative zonal current causes a positive surface stress anomaly and vice versa (a similar result is found for the meridional current, See Supplementary Fig. 2). The temporal correlation between zonal surface stress anomaly and zonal surface current over the entire simulation year reaches -0.8.

Further evidence for the influence of tides on surface stress is revealed by analysis of the zonal stress spectrum in mid-Channel in the year-long twin experiments (Fig. 3b). In CTRL, the surface stress spectrum is characterized by a well-defined peak at the tidal frequency M2. Similar results are found throughout the English Channel, i.e., where tidal currents are strong (See Supplementary Fig. 3).

A sink of tidal energy. To what extent do tides affect the exchange of energy between the ocean and the atmosphere, i.e., the wind work? To investigate this question, the wind work (FK) is estimated from the twin experiments as the product of the surface oceanic currents ($\mathbf{U}_o = (U_{ox}, V_{ox})$) and the surface stress ($\boldsymbol{\tau} = (\tau_x, \tau_y)$) ($FK = \frac{\overline{\mathbf{U}_o \cdot \boldsymbol{\tau}}}{\rho}$) and is illustrated for June in Fig. 2d. In NOCFB, the wind work is positive as generally expected if the atmosphere forces the ocean (See Supplementary Fig. 4). However, in CTRL over the English Channel, exactly at the locations of strong tidal currents, the positive FK is overwhelmed by an energy sink from the ocean to the atmosphere. Tides, through the feedback of tidal currents, create a conduit of energy from the ocean to the atmosphere. Part of the tidal energy in the ocean is therefore not dissipated by the bottom drag or internal tides, but by the top drag. To the best of our knowledge, this process is mentioned for the first time here. To shed more light on this energy sink, a co-spectral analysis of the wind work over a year is estimated in the middle of the Channel (Fig. 3c), with similar results over the English Channel (See Supplementary Fig. 3). The co-spectrum is estimated as $\Lambda = Re(\hat{\boldsymbol{\tau}} \cdot \widehat{\mathbf{U}}_o^*)$, where $\hat{\boldsymbol{\tau}}$ is the Fourier transform of the wind stress vector and $\widehat{\mathbf{U}}_o^*$ is the conjugate of the Fourier transform of the surface current vector. Note that a co-spectrum can have either positive or negative values as the autocovariances can be both positive and negative.

In both simulations, FK shows a positive energy input in almost the entire frequency range, which mainly represents Ekman current generation. Since mesoscale activity is low in the Channel, the currents are primarily wind-driven, explaining the

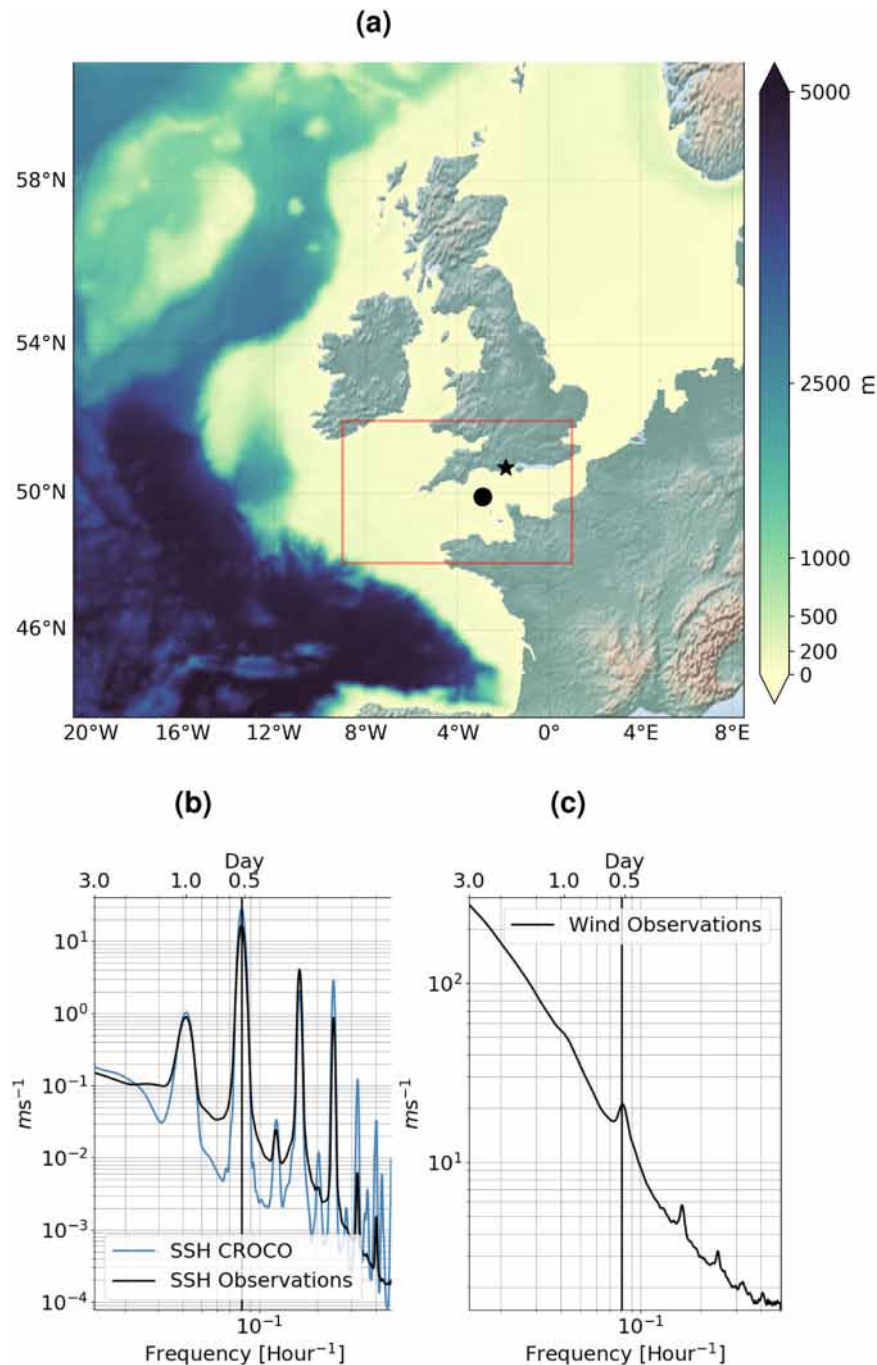


Fig. 1 The English Channel is home to some of the strongest and most complex tides in the World. **a** Domain configuration: the red rectangle frames the Channel and the region shown in Fig. 2; the black star (circle) highlights the location of the SSH (wind speed) measurement shown in **b** and **c**. **b** SSH Spectrum from the observations (black, 23-year) and from CROCO (blue, CTRL over 1-year). **c** Spectrum of in situ wind speed using 31-year. The vertical black lines highlight the M2 tidal frequency. A similar result can be found in other areas with high tides, for example in Alaska ("Drift River Terminal" station, see Supplementary Fig. 1).

small difference in positive wind work between the two simulations, even at mesoscale (100-day time scale). However, consistent with the previous analysis, a large negative peak appears in CTRL at M2, which can be unambiguously linked to the tidal current feedback to the atmosphere.

Current-induced tidal winds. The energy sink through top drag does not significantly affect the tidal currents (Fig. 3a for mid-Channel but similar results were over the English Channel, see Supplementary Fig. 2), which can be expected because it is

relatively small compared to the dissipation through bottom drag (about 0.5%). However, tidal winds generated by this mechanism are not negligible. To better understand this phenomenon, Fig. 2c presents a snapshot of the zonal wind anomaly estimated as the difference between the twin experiments. It shows a spatial pattern very similar to that of currents or surface stress anomaly: a negative zonal current causes a positive zonal surface stress and a negative wind work (energy input to the atmosphere), which in turn causes a positive zonal tidal wind (similar result is found for the meridional component but much weaker as the meridional

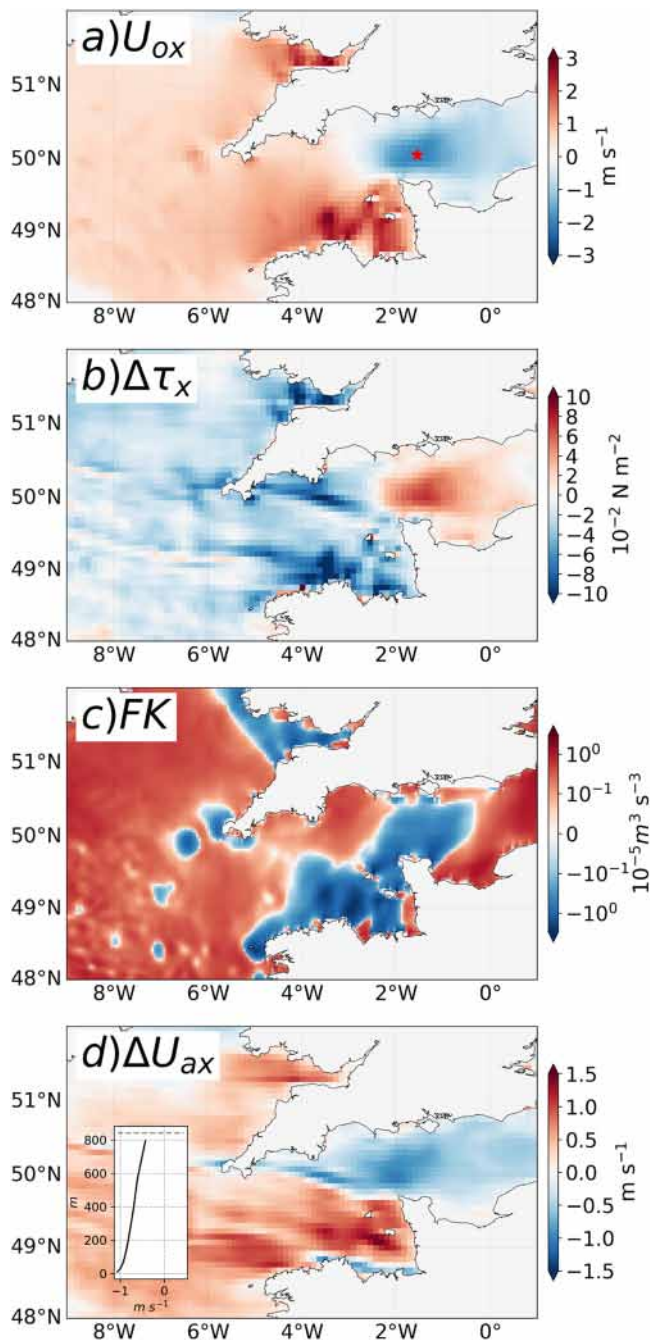


Fig. 2 Tidal currents modify the surface stress, inducing an energy sink and modifying the wind through the atmospheric boundary layer. The maps of the English Channel region show snapshots of the zonal surface currents and their effect on the surface airflow on 01/03/2020 at 15:30 UTC. Anomalies are estimated as the difference between CTRL and NOCFB. **a** Zonal tidal currents. **b** Surface zonal stress anomaly (a negative tidal current causes a positive surface stress anomaly). **c** Wind work (FK) during the month of June for CTRL; CFB causes a transfer of momentum from tidal currents to the atmosphere. **d** 10 m zonal wind zonal anomaly due to tidal current feedback (a negative tidal current causes a negative tidal wind); the inset shows the vertical profile of zonal winds at mid-Channel and the atmospheric boundary layer height indicated with a horizontal gray line.

current component is weaker, see Supplementary Fig. 2). The depth of the atmospheric boundary layer is not affected by tides. However, as shown in the vertical profile of wind anomaly (inset in Fig. 2c), the effect of tides can reach the top of the atmospheric

boundary layer (in the example shown, a stable layer of about 800 m) with a positive temporal correlation between currents and winds (>0.7 over a week). Above the atmospheric boundary layer, the correlation between currents and winds falls to insignificant values. The wind response is attenuated with height, consistent with a feedback effect acting at the air-sea interface and diffused aloft by vertical mixing²⁴. This tidal-frequency wind is evidenced by the temporal variations of wind anomaly. The correlation between zonal current and wind anomalies is 0.7 over the entire year and we found no time lag, indicating a rapid response of the atmosphere (less than an hour) to ocean tides. Spectral analysis of low-level winds in mid-Channel reveals a peak exactly at the M2 frequency in CTRL, not present in NOCFB (Fig. 3d). Similar results are found elsewhere over the English Channel (See Supplementary Fig. 3). These tidal winds can have amplitude greater than $1 m s^{-1}$. At this frequency, the currents are a source of energy for the wind and not the other way around.

In the literature, only two categories of atmospheric tides are documented: the gravitational tides (similar to oceanic tides) and the thermal tides, i.e., the effect of diurnal heating of air masses by the sun^{22,25}. These atmospheric tides are shown to be an important transport mechanism in the upper atmosphere²⁶. However, while they dominate the dynamics of the mesosphere and lower thermosphere, they are very weak in the troposphere. Yet their effect on pressure propagates to the surface and can add (by an inverse barometric effect) about 1 cm of elevation amplitude to the oceanic S2 tide—overall a small contribution to the tides. We demonstrate here the existence, to the best of our knowledge, of a new class of atmospheric tides induced by the drag of ocean tides.

Reference¹³ defined a coupling coefficient (s_w) between surface currents and low-level winds to characterize the wind response to mesoscale ocean eddies. Similarly, a statistical relationship can be found for tidal winds. Here, the coupling between 10 m winds and surface currents is evaluated by bin averaging the zonal current and wind anomalies between CTRL and NOCFB over the English Channel. Figure 4a shows the resulting scatterplot. It reveals a clear positive linear relationship between tidal current and wind, with s_w defined as the slope of the linear regression in the scatterplot. $s_w = 0.32$, i.e., the tidal wind amplitude is about 32% of the surface current amplitude, and thus can reach a couple of $m s^{-1}$. Without the influence of the currents, the surface stress anomalies have by definition a positive correlation with the wind anomalies. In CTRL, CFB has a bottom-up effect²⁴: a positive current anomaly causes a negative surface stress that in turn causes a positive wind anomaly. A similar result is found at mesoscale in Ref. ²⁴. The positive sign is therefore consistent with a negative surface stress response and a tidal energy sink and confirms that a positive zonal (meridional) tidal current causes a positive zonal (meridional) wind. Interestingly, s_w is very similar for the tides and the oceanic mesoscale (around 0.3 (Ref. ²⁴)).

Discussion

The same tidal wind generation mechanism is likely to be present around the global ocean for other tidal regimes and, in particular, in regions with strong tides such as Canada or Alaska. Although the current feedback effect must vary to some extent in space and time, a simple estimate of the global friction-induced tidal winds can be derived by factoring the M2 tidal currents from TPXO9-v5²⁷ by the coupling coefficient s_w . Figure 4b presents a global map of the estimated M2 tidal winds (similar results are found for other main constituents). Not surprisingly, it reveals the presence of tidal winds mainly in coastal areas with wide shelves, where tidal currents are strongest. According to this estimate, M2 tidal winds can reach up to $1.5 m s^{-1}$ near the islands of Alaska,

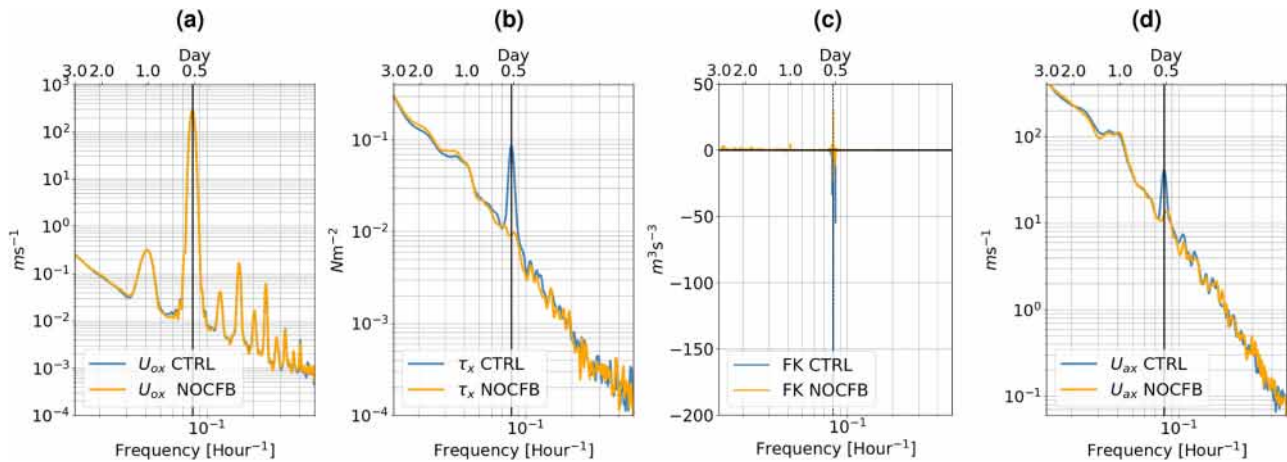


Fig. 3 Current feedback results in a tidal imprint on the surface stress, air-sea energy flux and wind spectra. Results from CTRL and NOCFB are shown for mid-Channel (red star in Fig. 2a): **a** Zonal current; **b** zonal surface stress; **c** co-spectrum (Λ) of the wind work. **d** 10 m zonal wind. In a, b, c, d a vertical line highlights the M2 tidal frequency.

Argentina, Norway and the Amazon. Note that this estimate based on a global tidal model probably underestimates the strong locally generated tidal currents expected around small-scale unresolved bathymetries.

The results presented in this study provide an opportunity to understand how ocean tides can be dissipated and, overall, how they interact with the atmosphere. M2 represents a total work rate of 2.4 TW³. A simple estimate of the M2 tidal energy sink to the atmosphere can be derived from this study. Here, the energy sink corresponds to about 0.5% of the dissipation by the bottom drag. Therefore, about 0.012 TW may be lost to the atmosphere by ocean tides. Tidal winds represent a non-trivial high-frequency wind regime. In an ocean-only model, they can be parameterized using the stress or wind correction approach proposed in¹⁷, although these parameterizations must be tested specifically for tidal frequencies.

In terms of scientific and societal impact, the expected reduction in wind biases associated with tidal winds over broad continental shelves should benefit climate modeling and weather forecasting, with applications for regular shipping, search and rescue services, and events such as regattas. It could also be relevant to environmental issues (e.g., oil spills) and to renewable energy from wind farms—wind power varying with the cube of the wind speed. As an illustration, if we consider an average wind speed of 6 ms⁻¹, a tidal wind of 1 ms⁻¹ would result in a 10% increase in offshore wind energy, a figure similar to the estimated effect of climate change²⁸.

Methods

The Coastal and Regional Ocean Community model (CROCO). The oceanic simulations were performed with CROCO²⁹, developed around the kernel of the Regional Oceanic Modeling System³⁰. CROCO is a free-surface, terrain-following coordinate model with split-explicit time stepping and Boussinesq and hydrostatic approximations are used in this study. The grid is centered around England and covers the English Channel, extending from 20°W to 8°E and from 43.3°N to 61°N; the grid size is 586×586 points and grid resolution is 2.7 km to 4.0 km. The bathymetry is constructed from the Shuttle Radar Topography Mission (SRTM30 plus) dataset (available at http://topex.ucsd.edu/WWW_html/srtm30_plus.html) based on the 1-min³¹ global dataset and higher-resolution data where available. To avoid aliasing and ensure smoothing of the topography at the grid scale, a Gaussian smoothing kernel with a width of 4 times the topographic grid spacing is applied. In addition, local topography smoothing (with $r = 0.2$) is applied to avoid pressure gradient errors induced by terrain-following coordinates on steep slopes³². 50 vertical levels are used with enhanced resolution at the surface, bottom and thermocline provided by stretching parameters: $\theta_s = 7$, $\theta_b = 2$ and $h_{cline} = 300$ m. The model is initialized using the daily averaged Global MERCATOR reanalysis GLORYS2V4³³, and is spun up as an ocean-only model for 1 year, using surface forcing from the

CFRS atmospheric reanalysis. It is then run as a coupled model for all of 2010 using interannual oceanic boundary forcing from daily GLORYS reanalysis.

Tidal simulation with CROCO has been validated many times^{34–36}, and tidal forcing is invariably performed as follows. At open boundaries, tidal data (elevation and barotropic currents) are interpolated from the Oregon State University global model of ocean tides TPXO²⁷, and applied through Flather-type conditions as for other barotropic currents³⁷. Because the computational domain covers a large basin, tidal potential is also applied as a body force in the interior (including direct astronomical contributions from the sun and moon, contributions from solid Earth body tide, self-attraction of ocean tides and load tides). The bottom drag is computed assuming a logarithmic law in the bottom boundary layer with a roughness length $Z_{ob} = 10^{-2}$ m. Finally, the K-profile parameterization (KPP)³⁸ is used for vertical mixing of tracers and momentum in the surface and bottom boundary layers and in the interior.

The Weather Research and Forecast model (WRF). WRF³⁹, version 4.1, is implemented on a slightly larger domain than CROCO to include it inside its sponge layers 4 points²⁰. The grid has a spatial resolution of ≈ 6 km. Initial and boundary conditions are derived from the Climate Forecast System Reanalysis⁴⁰, CFRS, which has a spatial resolution of about 40 km and is used for initialization on January 1st, 2010 and boundary forcing for 1 year. For parameterizations (boundary layer, convection, micro-physics, radiation etc), the reader is referred to¹⁹. In the boundary layer model, a bulk formula⁴¹ is used to compute the surface turbulent heat, freshwater and momentum fluxes, which are subsequently provided to CROCO. Note that to properly account for the impact of surface ocean currents on the atmosphere, we must also modify the tridiagonal matrix system solved in the vertical turbulent diffusion scheme^{42,43}.

Coupling experiments. Model data are exchanged hourly between CROCO and WRF through the OASIS3 coupler⁴⁴. In the control simulation (CTRL) of the twin experiments, WRF provides CROCO with hourly averages of freshwater, heat, and momentum fluxes, while CROCO returns the hourly average sea surface temperature. Current feedback (CFB) is considered by estimating the surface stress using the 10 m wind $\mathbf{U}_a = (U_{ax}, U_{ay})$ (which corresponds to the first vertical level in WRF) relative to the moving ocean surface $\mathbf{U}_o = (U_{ox}, U_{oy})$ (computed at the top vertical level in CROCO):

$$\mathbf{U} = \mathbf{U}_a - \mathbf{U}_o \quad (1)$$

The surface stress is then estimated as

$$\boldsymbol{\tau} = \rho_a C_D (\mathbf{U}_a - \mathbf{U}_o) |\mathbf{U}_a - \mathbf{U}_o| = \rho_a C_D \mathbf{U} |\mathbf{U}|. \quad (2)$$

where ρ_a is the surface air density and C_D the surface drag.

A second experiment called NOCFB is similar to CTRL except for the absence of current feedback to the atmosphere (CFB): the surface stress is estimated using the absolute wind \mathbf{U}_a rather than the relative wind \mathbf{U} and so:

$$\boldsymbol{\tau} = \rho_a C_D \mathbf{U}_a |\mathbf{U}_a|. \quad (3)$$

Note that an additional experiment with CFB but without tide leads to similar conclusions about friction-induced tidal winds.

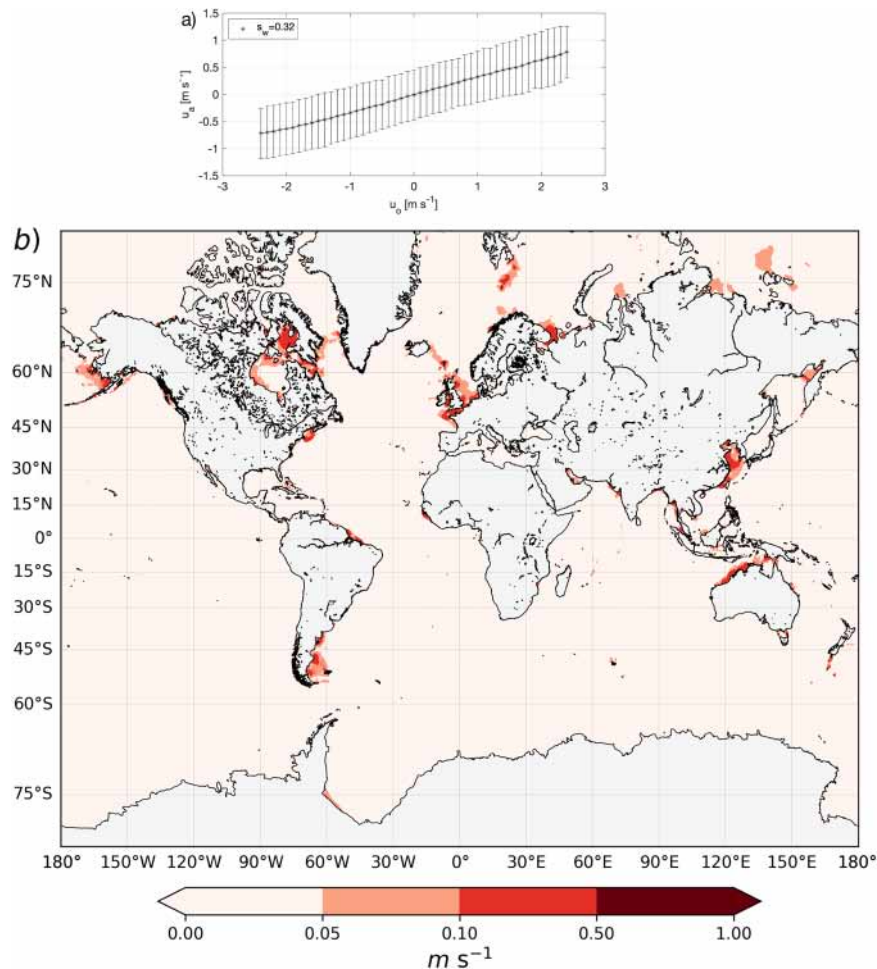


Fig. 4 Ocean tides modify the winds of the overlying atmosphere in broad-shelf coastal areas. a Binned scatterplot of the complete time series of the surface current and 10 m wind difference between CTRL and NOCFB over the English Channel. Bars indicate the standard deviation around the mean drawn by the stars. The linear regression is indicated by a black line and the slope s_w is given in the inset. **b** Global M2 tidal winds estimated by the M2 tidal currents of TPX09-v5 factored by s_w .

Data availability

The in situ data can be found on <http://www.marineinsitu.eu/>. Data used in the figures are available in https://figshare.com/articles/figure/Data_to_plot_Figures_from_Renault_et_al_2022_CFB_Tides/19153280

Code availability

CROCO and WRF are free softwares distributed in <https://www.croco-ocean.org/> and <https://github.com/wrf-model/WRF>.

Received: 15 December 2021; Accepted: 2 March 2022;

Published online: 25 March 2022

References

- Munk, W. & Wunsch, C. Abyssal recipes ii: energetics of tidal and wind mixing. *Deep Sea Res.* **45**, 1977–2010 (1998).
- Wunsch, C. & Ferrari, R. Vertical mixing, energy, and the general circulation of the oceans. *Annu. Rev. Fluid Mech.* **36**, 281–314 (2004).
- Le Provost, C. & Lyard, F. Energetics of the M2 barotropic ocean tides: an estimate of bottom friction dissipation from a hydrodynamic model. *Prog. Oceanogr.* **40**, 37–52 (1997).
- Egbert, G. D. & Ray, R. D., Semi-diurnal and diurnal tidal dissipation from topex/poseidon altimetry. *Geophys. Res. Lett.* **30**, <https://doi.org/10.1029/2003GL017676> (2003).
- Egbert, G. & Ray, R. Significant dissipation of tidal energy in the deep ocean inferred from satellite altimetry data. *Nature* **405**, 775–778 (2000).
- Mathur, M., Carter, G. S. & Peacock, T. Topographic scattering of the low-mode internal tide in the deep ocean. *J. Geophys. Res.* **119**, 2165–2182 (2014).
- Stammer, D. Global characteristics of ocean variability estimated from regional topex/poseidon altimeter measurements. *J. Phys. Oceanogr.* **27**, 1743–1769 (1997).
- Dubley, C. B., Schlax, M. G. & Samelson, R. M. Summertime coupling between sea surface temperature and wind stress in the California current system. *J. Phys. Oceanogr.* **37**, 495–517 (2007).
- Mc. Williams, J. C. The nature and consequences of oceanic eddies. *Geophys. Monograph Series* **177**, 5–15 (2008).
- Luo, J. J., Masson, S., Roeckner, E., Madec, G. & Yamagata, T. Reducing climatology bias in an ocean-atmosphere cgm with improved coupling physics. *J. Climate* **18**, 2344–2360 (2005).
- Pacanowski, R. Effect of equatorial currents on surface stress. *J. Phys. Oceanogr.* **17**, 833–838 (1987).
- Renault, L., Molemaker, M. J., Gula, J., Masson, S. & Mc. Williams, J. C. Control and stabilization of the gulf stream by oceanic current interaction with the atmosphere. *J. Phys. Oceanogr.* **46**, 3439–3453 (2016).
- Renault, L. et al. Modulation of wind work by oceanic current interaction with the atmosphere. *J. Phys. Oceanogr.* **46**, 1685–1704 (2016).
- Seo, H., Miller, A. J. & Norris, J. R. Eddy–wind interaction in the California current system: dynamics and impacts. *J. Phys. Oceanogr.* **46**, 439–459 (2016).
- Renault, L., Mc. Williams, J. C. & Gula, J. Dampening of submesoscale currents by air–sea stress coupling in the californian upwelling system. *Sci. Rep.* **8**, 13388 (2018).
- Jullien, S. et al. Impact of ocean–atmosphere current feedback on the ocean mesoscale activity: regional variations, and sensitivity to model resolution. *J. Clim.* **33**, 2585–2602 (2020).

17. Renault, L., Masson, S., Arsouze, T., Madec, G. & Mc. Williams, J. C. Recipes for how to force oceanic model dynamics. *J. Adv. Model. Earth Syst.* **12**, e2019MS001715 (2020).
18. Renault, L., Arsouze, T. & Ballabrera-Poy, J. On the influence of the current feedback to the atmosphere on the western mediterranean sea dynamics. *J. Geophys. Res.* **126**, e2020JC016664 (2021).
19. Renault, L., Mc. Williams, J. C. & Penven, P. Modulation of the agulhas current retroreflection and leakage by oceanic current interaction with the atmosphere in coupled simulations. *J. Phys. Oceanogr.* **47**, 2077–2100 (2017).
20. Renault, L., Marchesiello, P., Masson, S. & Mc. Williams, J. C. Remarkable control of western boundary currents by eddy killing, a mechanical air-sea coupling process. *Geophys. Res. Lett.* **46**, 2743–2751 (2019).
21. Dewar, W. K. & Flierl, G. R. Some effects of the wind on rings. *J. Phys. Oceanogr.* **17**, 1653–1667 (1987).
22. Green, J. S. A. Atmospheric tidal oscillations: an analysis of the mechanics. *Proc. R. Soc. Lond. Ser. A* **288**, 564–574 (1965).
23. Fornerino, M. & Provost, C. L. A model for prediction of the tidal currents in the english channel. *Int. Hydrogr. Rev.* **0**, 143–166 (1985).
24. Renault, L., Masson, S., Oerder, V., Jullien, S. & Colas, F. Disentangling the mesoscale ocean-atmosphere interactions. *J. Geophys. Res.* **124**, 2164–2178 (2019).
25. Chapman, S. Atmospheric tides and oscillations in Compendium of Meteorology. 510–530 (Springer, 1951).
26. Forbes, J. et al. Tidal variability in the ionospheric dynamo region. *J. Geophys. Res. Space Phys.* **113**, <https://doi.org/10.1029/2007JA012737> (2008).
27. Egbert, G. D. & Erofeeva, S. Y. Efficient inverse modeling of barotropic ocean tides. *J. Atmos. Oceanic Technol.* **19**, 183–204 (2002).
28. Zeng, Z. et al. A reversal in global terrestrial stilling and its implications for wind energy production. *Nat. Clim. Change* **9**, 979–985 (2019).
29. Debreu, L., Marchesiello, P., Penven, P. & Cambon, G. Two-way nesting in split-explicit ocean models: algorithms, implementation and validation. *Ocean Modelling* **49**, 1–21 (2012).
30. Shchepetkin, A. F. & Mc. Williams, J. C. The Regional Oceanic Modeling System (ROMS): a split-explicit, free-surface, topography-following-coordinate oceanic model. *Ocean Modelling* **9**, 347–404 (2005).
31. Sandwell, D. T. & Smith, W. H. F. Marine gravity anomaly from Geosat and ERS 1 satellite altimetry. *J. Geophys. Res. Solid Earth* **102**, 10039–10054 (1997).
32. Beckmann, A. & Haidvogel, D. B. Numerical simulation of flow around a tall isolated seamount. part i: Problem formulation and model accuracy. *J. Phys. Oceanogr.* **23**, 1736–1753 (1993).
33. Ferry, N. et al. Gloryst2v1 global ocean reanalysis of the altimetric era (1992–2009) at meso scale. *Mercator Ocean–Quarterly Newsletter* **44** (2012).
34. Blaas, M., Dong, C., Marchesiello, P., Mc. Williams, J. C. & Stolzenbach, K. Sediment-transport modeling on southern californian shelves: a ROMS case study. *Continental Shelf Res.* **27**, 832–853 (2007).
35. Minh, N. N. et al. Tidal characteristics of the gulf of tonkin. *Continental Shelf Res.* **91**, 37–56 (2014).
36. Marchesiello, P. et al. Erosion of the coastal mekong delta: assessing natural against man induced processes. *Continental Shelf Res.* **181**, 72–89 (2019).
37. Marchesiello, P., Mc. Williams, J. C. & Shchepetkin, A. Open boundary conditions for long-term integration of regional oceanic models. *Ocean Modelling* **3**, 1–20 (2001).
38. Large, W. G., Mc. Williams, J. C. & Doney, S. C. Oceanic vertical mixing: a review and a model with a nonlocal boundary layer parameterization. *Rev. Geophys.* **32**, 363–404 (1994).
39. Skamarock, W., Klemp, J., Dudhia, J., Gill, D., Barker, D. A description of the Advanced Research WRF version 3. NCAR, (Note NCAR/TN-4751STR), Technical report (2008).
40. Saha, S. et al. The NCEP climate forecast system reanalysis. *Bull. Am. Meteorol. Soc.* **91**, 1015–1057 (2010).
41. Fairall, C., Bradley, E. F., Hare, J., Grachev, A. & Edson, J. Bulk parameterization of air-sea fluxes: updates and verification for the coare algorithm. *J. Clim.* **16**, 571–591 (2003).
42. Lemarié, F. Numerical modification of atmospheric models to include the feedback of oceanic currents on air-sea fluxes in ocean-atmosphere coupled models, (INRIA Grenoble - Rhône-Alpes; Laboratoire Jean Kuntzmann; Université de Grenoble I - Joseph Fourier; INRIA), Technical Report RT-464 (2015).
43. Renault, L., Lemarié, F. & Arsouze, T. On the implementation and consequences of the oceanic currents feedback in ocean-atmosphere coupled models. *Ocean Modelling* **0**, 101423 (2019).
44. Valcke, S. The oasis3 coupler: a european climate modelling community software. *Geosci. Model Dev.* **6**, 373–388 (2013).

Acknowledgements

This work used GENCI computing resources projects 7298 and 13051. We appreciate support from the CNES (Projects CARAMBA and I_CASCADE), the ANR JPI-CLIMATE EUREC4A-OA, the NOAA project ATOMIC, and the GdR (CNRS) and GdRI (IRD) CROCO. We thank S. Masson for useful discussions.

Author contributions

L.R. designed research; L.R. and P.M. analyzed data and model output; L.R. and P.M. wrote the paper.

Competing interests

The authors declare no competing interests.

Additional information

Supplementary information The online version contains supplementary material available at <https://doi.org/10.1038/s43247-022-00403-y>.

Correspondence and requests for materials should be addressed to Lionel Renault.

Peer review information Communications Earth & Environment thanks the anonymous reviewers for their contribution to the peer review of this work. Primary Handling Editor: Heike Langenberg.

Reprints and permission information is available at <http://www.nature.com/reprints>

Publisher's note Springer Nature remains neutral with regard to jurisdictional claims in published maps and institutional affiliations.



Open Access This article is licensed under a Creative Commons Attribution 4.0 International License, which permits use, sharing, adaptation, distribution and reproduction in any medium or format, as long as you give appropriate credit to the original author(s) and the source, provide a link to the Creative Commons license, and indicate if changes were made. The images or other third party material in this article are included in the article's Creative Commons license, unless indicated otherwise in a credit line to the material. If material is not included in the article's Creative Commons license and your intended use is not permitted by statutory regulation or exceeds the permitted use, you will need to obtain permission directly from the copyright holder. To view a copy of this license, visit <http://creativecommons.org/licenses/by/4.0/>.

© The Author(s) 2022